Dynamics of a Simulated North American Monsoon Gulf Surge Event

ANDREW J. NEWMAN* AND RICHARD H. JOHNSON

Department of Atmospheric Science, Colorado State University, Fort Collins, Colorado

(Manuscript received 4 October 2012, in final form 6 March 2013)

ABSTRACT

Gulf surges are transient disturbances that propagate along the Gulf of California (GoC) from south to north, transporting cool moist air toward the deserts of northwest Mexico and the southwest United States during the North American monsoon. They have been shown to modulate precipitation and have been linked to severe weather and flooding in northern Mexico and the southwest United States. The general features and progression of surge events are well documented but their detailed dynamical evolution is still unclear. In this study, a convection-permitting simulation is performed over the core monsoon region for the 12–14 July 2004 gulf surge event and the dynamics of the simulated surge are examined. Initially, convection associated with the tropical easterly wave precursor to Tropical Cyclone Blas creates a disturbance in the southern GoC on early 12 July. This disturbance is a precursor to the gulf surge on 13 July and is a *Kelvin shock* (internal bore under the influence of rotation) that dissipates in the central GoC. The surge initiates from inflow from the mouth of the GoC along with convective outflow impinging on the southern GoC. Continued convective outflow along the GoC generates multiple gravity currents and internal bores while intensifying the simulated surge as it propagates up the GoC. As the core of the surge reaches the northern GoC, a Kelvin shock is again the best dynamical fit to the phenomenon. Substantial low-level cooling and moistening are associated with the modeled surge along the northern GoC as is observed.

1. Introduction

Gulf surge events, or surge events for short, are critical transient events in the North American monsoon (NAM) because they have been tied to moisture flux and precipitation anomalies during the NAM (Anderson et al. 2000a; Berbery 2001; Douglas and Leal 2003; Gochis et al. 2004; Higgins et al. 2004) and severe weather outbreaks in Arizona (Maddox et al. 1995). Most of the large-scale features associated with the initiation of a surge event were first identified over 35 years ago and have come to a consensus in the literature. Hales (1972) and Brenner (1974) first introduced the concept of a "surge" of cool moist air providing moisture to the monsoon region from the tropical east Pacific channeled through the Gulf of California (GoC). Hales (1972) describes several surge events and typical characteristics associated with them. It was also noted that surges are generally associated with some type of cloudy disturbance south of the GoC as shown in satellite imagery (Hales 1972). Brenner (1974) highlights one surge case and notes that easterly waves, tropical cyclones, or some other agent could initiate a surge event. Figure 1 gives a general overview of the NAM region with some relevant features of the surge event examined herein.

More recently, modeling and statistical studies have been performed to determine the causes and evolution characteristics of surge events (Stensrud et al. 1997; Fuller and Stensrud 2000; Anderson et al. 2000b; Higgins and Shi 2005; Adams and Stensrud 2007). Fuller and Stensrud (2000) show that tropical easterly waves (TEWs) are precursors to many surges while Higgins and Shi (2005) show that tropical cyclones (TCs) moving near the mouth of the GoC lead to a higher occurrence of strong surges. The Madden–Julian oscillation may even modulate surge events through its modulation on eastern Pacific tropical cyclone genesis (Maloney and Hartmann 2000). Bordoni and Stevens (2006) use principal component analysis to show that a gulf surge mode is the

* Current affiliation: National Center for Atmospheric Research,[+] Boulder, Colorado.

[+] The National Center for Atmospheric Research is sponsored by the National Science Foundation.

Corresponding author address: Andrew Newman, National Center for Atmospheric Research, Boulder, CO 80307.
E-mail: anewman@ucar.edu

DOI: 10.1175/MWR-D-12-00294.1

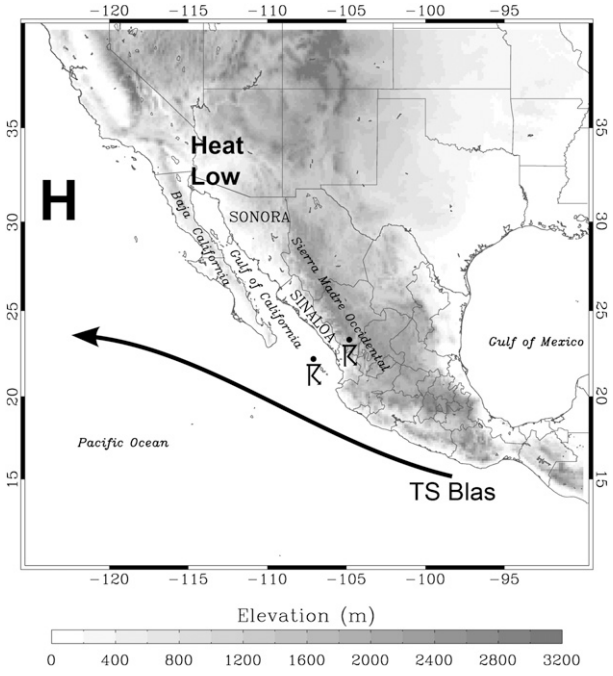

FIG. 1. Overview of the NAM region during the 12–14 Jul 2004 surge event. Geographic and political boundaries are noted. The black line indicates the general path of Tropical Storm Blas, ''heat low'' indicates the position of surface heat low in desert southwest United States, while the Pacific surface high pressure center is indicated by ''H''. Thunderstorm symbols indicate general area of convection thought to initiate surge events in Stensrud et al. (1997).

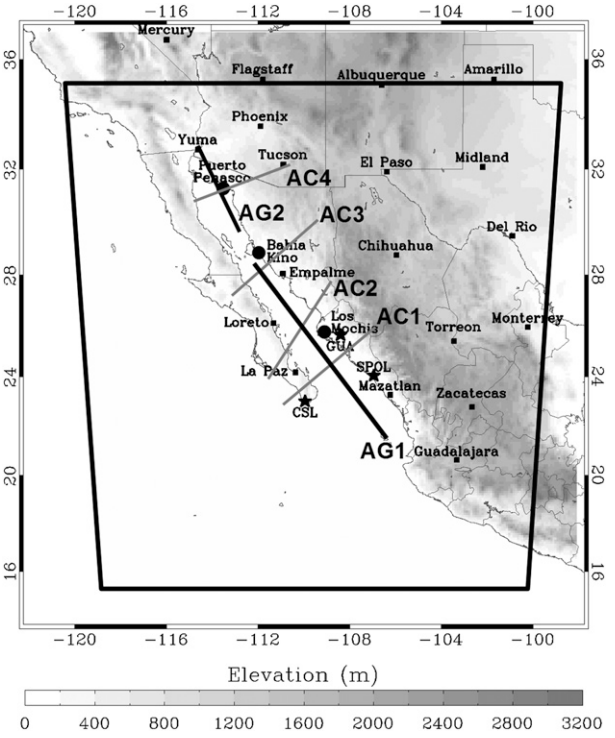

FIG. 2. Core NAM region with the model domain outlined (trapezoid). Also depicted are the three ISS sites (large circles): Puerto Penasco (PP), Bahia Kino (BK), and Los Mochis (LM). AG1, AG2, AC1, AC2, AC3, and AC4 denote the along-gulf and across-gulf cross-sectional locations, respectively.

leading EOF in the region during the NAM season and that it relates strongly to TEW passage. The modeling studies of Stensrud et al. (1997) and Adams and Stensrud (2007) again show that TEWs are associated with surge events in some manner.

However, there are a few important aspects of surge events that are still unresolved. The largest unknown pertains to the dynamics of surge events and their evolution. Since the events occur in a data-sparse region, it has been difficult to unravel what type of phenomenon a surge event is and whether it evolves from one type of system to another (i.e., gravity current to solitary wave) during its life cycle. Zehnder (2004) examines a detailed list of possible dynamical mechanisms for surge events, but does not come to a definitive conclusion. Rogers and Johnson (2007, hereafter RJ07), look at one strong surge event from an observational standpoint and conclude that an internal bore is the most likely suspect for the initial surge event. Mejia et al. (2010) examine the same surge using aircraft data but cannot reach a definitive conclusion regarding the surge dynamics. Overall, it is generally thought that gulf surges are likely some type of coastally trapped disturbance (Zehnder 2004; RJ07), but the specific dynamical definition of surge events remains unclear.

To attempt to more definitively answer what a surge event is and how it evolves dynamically, a model simulation of a surge event that occurred during the North American Monsoon Experiment (NAME; Higgins et al. 2006) is examined. This simulation is compared in detail to NAME observations in Newman and Johnson (2012, hereafter NJ12) and shows the ability to reproduce observed features of the surge event in a very reasonable manner. The dynamics of the simulated surge will be discussed to provide a clearer picture of the surge from initiation through its arrival in the Sonoran Desert. A brief description of the model configuration is followed by an assessment of the dynamics of the simulated surge and finally, a summary discussion.

2. Model configuration

The Weather Research and Forecasting Model (WRF), Advanced Research WRF (ARW) dynamical core version 3.2.1, was used in this study (Bruyere et al. 2010). One high-resolution domain (Fig. 2) was used with a

domain size of 2000 km × 2320 km and a horizontal grid spacing of 4-km (501 × 581 points) and 55 vertical levels between the surface and 100 hPa. The vertical grid is stretched such that it has seven levels in the lowest 1 km to a constant Δz of ~340 m in the upper troposphere. This horizontal resolution allows explicit simulation of convective systems, not necessarily convective elements, thus it can be considered convection permitting (Bryan and Morrison 2012) and no convective parameterization is used. In all simulations the Rapid Radiative Transfer Model longwave, Dudhia shortwave, Thompson et al. (2008) microphysics (with bug fixes to graupel calculations), Noah land surface model, and quasi-normal scale elimination (QNSE) surface and boundary layer schemes are used (Sukoriansky et al. 2006). The North American Regional Reanalysis (NARR; Mesinger et al. 2006) was used for initial and boundary conditions and the simulation was initialized at 1200 UTC 11 July and integrated until 0000 UTC 14 July. All analysis begins at 0600 UTC 12 July giving 18 h of spinup time for WRF to generate the appropriate higher resolution circulations and precipitation features. See NJ12 for further discussion of the model configuration.

3. Dynamical mechanisms

In an attempt to answer the unresolved question of the dynamical mechanism of the gulf surge, possible theoretical phenomena are compared to the simulated surge feature. Coastally trapped disturbances (CTDs) are disturbances that propagate along topographic barriers that are parallel to the coastline (Durran 2000). They are characterized by being rotationally trapped against the topography by Coriolis effects and their amplitude decays away from the coastline (Skamarock et al. 1999; Durran 2000). The wave amplitude also decays in the vertical as the CTD is vertically trapped with the trapping mechanism discussed shortly. Many past studies have examined CTDs over various regions of the world and have characterized CTDs as some type of laterally trapped linear Kelvin wave (with the topography on the right in the Northern Hemisphere), a Kelvin wave modified by a topographically trapped Rossby wave, a Kelvin wave that has nonlinearly steepened into a shock front on the leading edge, or a rotating gravity current (Gill 1977; Dorman 1985; Holland and Leslie 1986; Dorman 1987; Mass and Albright 1987; Reason and Steyn 1992; Rogerson and Samelson 1995; Skamarock et al. 1999; Ralph et al. 2000; Durran 2000; Zehnder 2004; RJ07). It is also possible the surge is an internal bore or gravity current that is propagating up the GoC with no rotational impacts and therefore not coastally trapped. Thus, there are many plausible dynamical mechanisms of which the following will be examined herein: gravity currents with/without rotation, internal bores, internal bores with rotation (or Kelvin shocks), topographically trapped Rossby waves, or some type of coastally trapped Kelvin wave (Gill 1982; Reason and Steyn 1992; Federov and Melville 1996; Skamarock et al. 1999; Helfrich et al. 1999; Durran 2000; Ralph et al. 2000; Zehnder 2004).

Before delving into the dynamics of the gulf surge event, some background discussion on Kelvin wave and Kelvin shock type CTDs is necessary. In the vertical, a Kelvin wave type CTD was assumed to be trapped by a strong marine layer inversion present above the boundary layer, which allows for use of the shallow-water model to explain the dynamics of the CTD (Gill 1977; Dorman 1985; Holland and Leslie 1986; Reason and Steyn 1992; Durran 2000). However, Durran (2000) showed that the vertical trapping mechanism of Kelvin wave type CTDs is actually that the CTDs are subinertial and that the terrain is of finite height. A subinertial wave is merely a wave with an angular frequency less than Coriolis (Durran 2000). For a Kelvin wave to be trapped by the marine layer inversion, the CTD wavelength would need to be typically less than ~5 km (Durran 2000). Durran (2000) goes on to term these Kelvin waves as ''step-trapped Kelvin waves'' and shows that they are dispersive with phase speed depending on wavelength and also the barrier height and atmospheric stratification. The shallow-water system predicts nondispersive Kelvin waves, trapped by the marine layer inversion suggesting that it may not be a good proxy for Kelvin wave type CTDs (Durran 2000). Therefore, discussion in this study will focus mainly on step-trapped Kelvin waves when examining the Kelvin wave gulf surge dynamical mechanism.

The term Kelvin shock is introduced by Helfrich et al. (1999) who study nonlinear fluid intrusions via a dam break in a rotating channel with a nonzero downstream depth. Kelvin shocks are essentially internal bores modified by rotation. They are characterized by having the maximum amplitude at the coast, limited offshore distance, across-coast velocities, and propagation speeds very similar to nonrotating internal bores. The shock front can also lag behind the leading edge at the coast depending on channel width and downstream fluid depth (Helfrich et al. 1999). These Kelvin shocks also transport fluid downstream, an important consideration for gulf surge events (Zehnder 2004). Finally, Kelvin shocks and Kelvin wave type CTDs will have isentropes that intersect the topography, an important distinction between them and topographically trapped Rossby waves (Zehnder 2004).

Two features, a precursor wave on 12 July 2004 and the initial surge impulse on 13 July are examined in the context of the above dynamical mechanisms. The

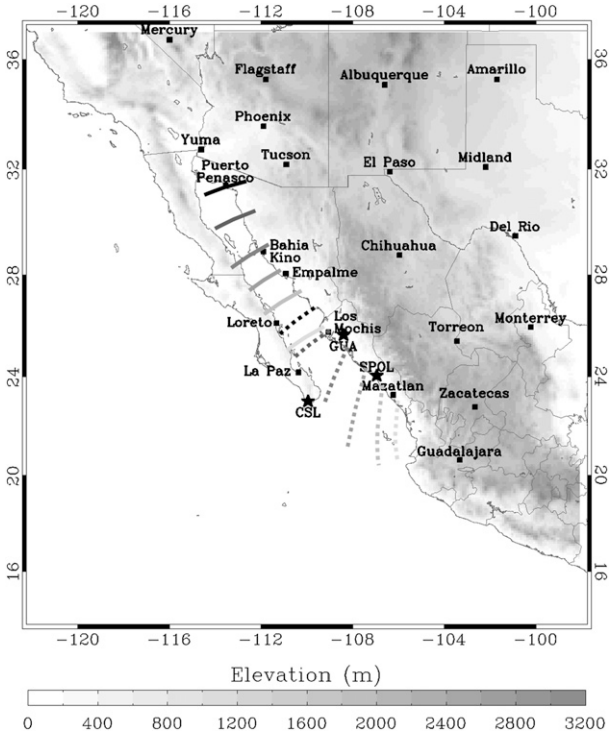

FIG. 3. Progression of the leading edge of S2 and the gulf surge in the simulation. Times depicted are 1000, 1200, 1400, 1600, 1800, and 2000 UTC 12 Jul for S2 (dashed lines) and 0300, 0500, 0700, 0900, 1100, and 1300 UTC 13 Jul for the gulf surge (solid lines). The lines progress from light to dark in chronological order.

simulated precursor wave is generated from a convective cluster related to the precursor tropical wave to Tropical Storm Blas near the mouth of the GoC just before 1000 UTC 12 July. This wave then propagates up the GoC through ~2000–2200 UTC washing out between Los Mochis (LM) and Bahia Kino (BK; NJ12). Figure 3 gives approximate leading edge locations for the precursor wave at various times on 12 July. The simulated gulf surge forms early on 13 July and then propagates up the GoC, reaching the northern GoC coastline after 1200 UTC (Fig. 3) (NJ12). The evolution of the surge is complex and will be discussed in more detail in later sections.

a. Precursor wave

1) INITIATION PHASE

The observed and simulated precursor wave on 12 July is thoroughly described in Mejia et al. (2010) and NJ12. Relevant to this work, the simulated wave originates from a convectively generated gravity current interacting with the mean stratification over the southern GoC (Fig. 4) (NJ12). This precursor wave is noted as "structure 2" (S2), while "structure 1" (S1) is defined as the convectively generated gravity current in Mejia et al. (2010) and herein. This generation mechanism immediately rules out topographically trapped Rossby waves. Topographically trapped Rossby waves are larger-scale features (~1500-km wavelength) generated by extended periods of downslope, offshore flow interacting with the ambient atmospheric stratification (Skamarock et al. 1999). In this case the gravity current interacts with the mean stratification over a period of only several hours over the GoC, thus void of an extended downsloping event. Furthermore, the wavelength of S2 is approximately ~700 km,[1] much less than that of the topographically trapped Rossby waves generated in Skamarock et al. (1999) or simulated by Zehnder (2004).

2) MATURE PHASE

S2 propagates along the GoC and moves ahead of S1 as S1 dissipates (Fig. 4, bottom). The modeled average total system speed from 1200 to 2000 UTC 12 July is $17.7 \pm 1.8\,\mathrm{m\,s^{-1}}$. A mass-weighted vertical average of the flow in the region just ahead of S2 is $1.6 \pm 0.5\,\mathrm{m\,s^{-1}}$ in the direction of propagation of S2 resulting in a modeled intrinsic phase speed of $16.1 \pm 1.9\,\mathrm{m\,s^{-1}}$. As S2 passes (starting at 1530 UTC) LM mean sea level pressure (MSLP) rises in phase with wind speed while the 2-m temperature also increases slightly (not shown). Above the surface, a shift to southerly or southeasterly winds (and thus moisture flux) and cooling is present behind the leading edge of S2 (Fig. 4, top). The top of S2 roughly aligns with the height of the Sierra Madre Occidental (SMO), the maximum wind magnitudes are at the coast and the flow is nearly parallel with the coast, but cross-coast flow (toward the SMO) is present throughout the passage of S2 (Fig. 5). Finally, there is no clear mixed layer capped with an inversion in the lowest 200 hPa, rather the atmosphere is continuously stratified with a Brunt–Väisälä frequency of $\sim 0.015\,\mathrm{s^{-1}}$.

From these characteristics, S2 is clearly not a gravity current with or without rotation. The question then is what is this phenomenon? Is it a coastally trapped Kelvin wave that can be described by the shallow-water system (Reason and Steyn 1992), a step-trapped Kelvin wave (Durran 2000), an internal bore (e.g., Klemp et al. 1997), a Kelvin shock (Helfrich et al. 1999), or some combination of these mechanisms? S2 propagates ahead of S1, with little surface cooling evident in Figs. 4 and 5 or at LM. Also, using Fig. 4 the estimated maximum phase speed of S1 is $\sim 12.5\,\mathrm{m\,s^{-1}}$ [$g' \approx 0.13\,\mathrm{m\,s^{-2}}$, $h \approx 600\,\mathrm{m}$,

[1] Estimated from an approximate 6-h passage time at Los Mochis and an $16\,\mathrm{m\,s^{-1}}$ phase speed resulting in a half wavelength of ~350 km [following Durran (2000)].

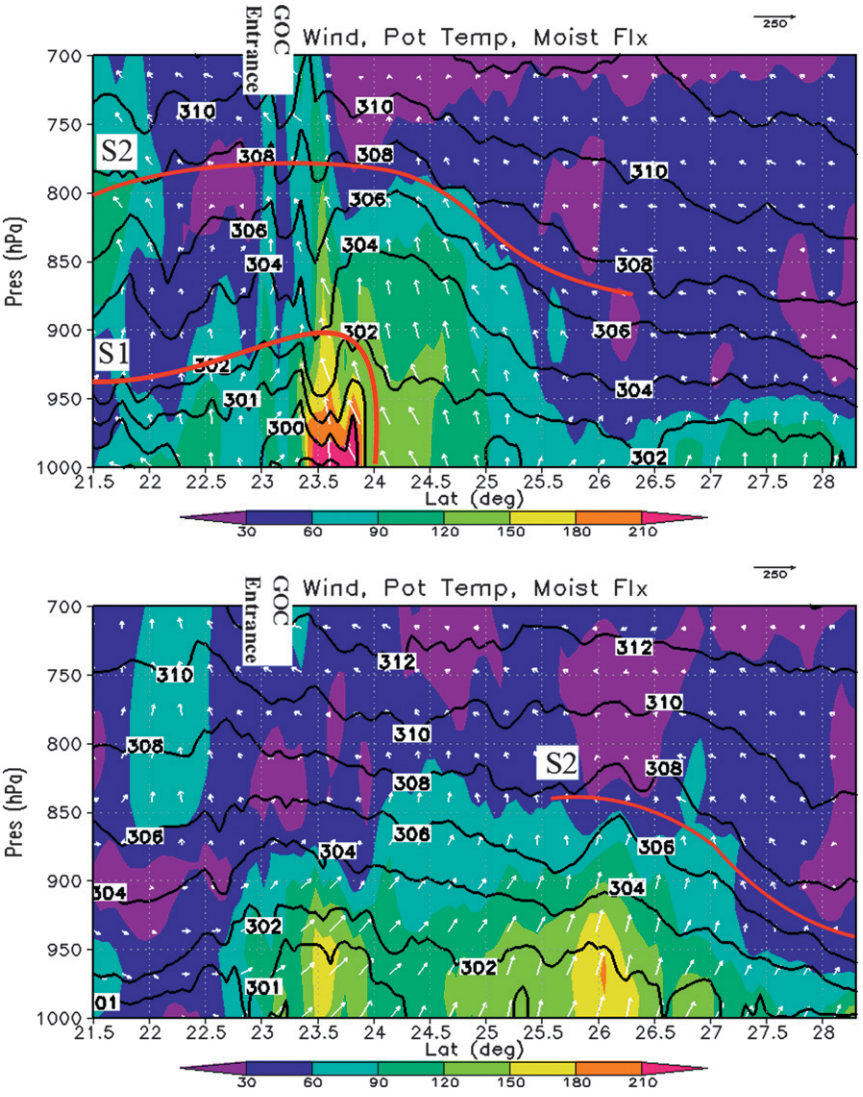

FIG. 4. Potential temperature (K, black lines), moisture flux (g m kg^{-1} s^{-1}, shading), and coast-relative moisture flux vectors (arrows) at (top) 1600 and (bottom) 2000 UTC 12 Jul 2004 along AG1 (Fig. 2). S1 denotes the cold pool associated with convection near the GoC entrance, and S2 denotes a deeper disturbance discussed in Mejia et al. (2010). Red lines give general boundaries of S1 and S2.

where $g' = g(\Delta\theta/\theta_o)$; Benjamin 1968], thus S2 is not a continuation of or tied to S1. In regards to coastally trapped Kelvin waves, the estimated wavelength of 700 km along with the absence of a clear mixed layer inversion, suggests the classic shallow-water description of Kelvin waves will not adequately describe the characteristics of S2 as this wave will not be trapped by an inversion layer (Durran 2000). Even with the presence of a large boundary layer inversion, the wavelength of S2 along with the mean Brunt–Väisälä frequency of 0.015 s^{-1} means the inversion will be unable to vertically trap S2 (Durran 2000). Using a representative height of ~1500 m for the SMO along the southern and central GoC, a phase speed of ~8.5 m s^{-1} for a linear step-trapped Kelvin wave could be expected (Durran 2000), around half of the model estimated phase speed. Also, there is across-coast flow present in S2 (Fig. 5) below the top of the SMO, which is excluded from analysis of linear step-trapped Kelvin waves (Durran 2000). Also note that the wavelength of S2 results in an angular frequency of $\omega_{s2} \approx 1.4 \times 10^{-4}$ s^{-1}, larger than f at 30°N (7.3×10^{-5} s^{-1}). Thus, it is unlikely that S2 is a step-trapped Kelvin wave.

Internal bores without rotation or Kelvin shocks are the other possible dynamical mechanisms for S2. For internal bores without rotation, Klemp et al. (1997) extended the work of Rottman and Simpson (1989) to

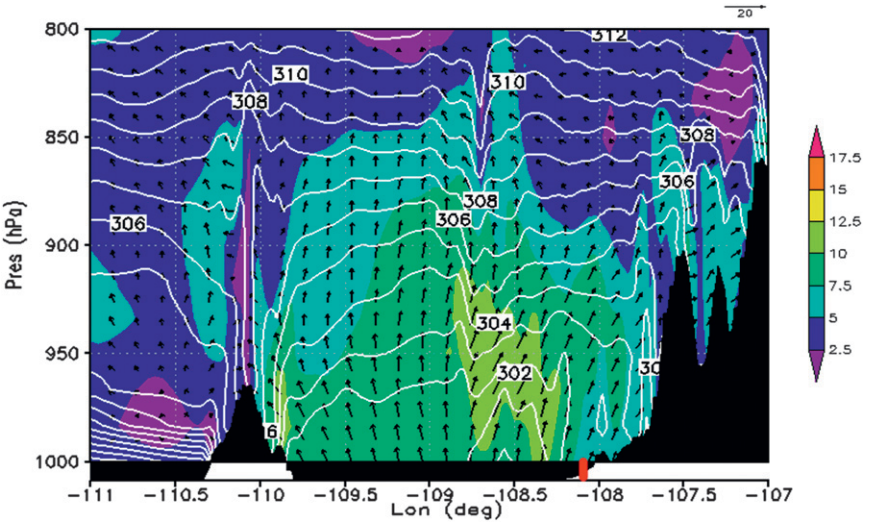

FIG. 5. Simulated potential temperature (K, white contours), wind magnitude ($m\,s^{-1}$, shading), and coast-relative wind vectors (arrows) along across-gulf cross section AC1 (Fig. 2) at 1730 UTC 12 Jul. Black shading indicates topography, while the red line indicates the coastline.

develop an improved phase speed relationship for internal bores within the shallow-water system that agrees very well with observations. Estimates of four parameters are needed: the pre- and postdisturbance height as well an estimate of the reduced gravity, which requires two potential temperature values. For S2 the 308 K (θ_2) isentrope is used as the best estimate for the top of S2 (Fig. 4, top), which gives a predisturbance height H_1 of 1500 m and a postdisturbance height H_2 of 1750 m. The mass-weighted potential temperature of the layer below θ_2 is 304.1 K (θ_1). These values and uncertainty estimates are summarized in Table 1. Uncertainty estimates for θ_1 and θ_2 are simply ± 0.5 K, while height estimates are calculated by taking the mean of the pre- and postdisturbance heights over a span of 2 h for the isentropes spanning the θ_1 and θ_2 uncertainty estimates. The standard deviation of the mean height is used as the uncertainty estimate. The phase speed of an internal bore is (Klemp et al. 1997)

$$C_B = [g' 2H_2^2/(H_1 + H_2)]^{1/2}, \quad (1)$$

where g' is reduced gravity given by

$$g' = g[(\theta_2 - \theta_1)/\theta_2]. \quad (2)$$

The theoretical phase speed if S2 is an internal bore is: $C_B \approx 15.3 \pm 1.6\,m\,s^{-1}$. The uncertainty for the theoretical phase speeds is the range using the fastest and slowest combination of parameter values in Table 1. The model estimated phase speed of S2 is slightly faster than that of an internal bore, but is within the uncertainty bounds and agrees the best with all possible dynamical options for the phenomenon. Knupp (2006) observes a gravity current through the generation of a leading internal bore to the dissipation of the gravity current and remaining solitary wave. This evolution is very similar to that of S2, which is generated by a gravity current, transitions to a mature bore with a dissipating gravity current, and finally dissipates hours after the dissipation of the generating gravity current (Fig. 4). However, an internal bore without rotation does not explain the maximum perturbation heights and velocities near the coast as is simulated (Fig. 5). Therefore, the dynamics of an internal bore without rotation does not fully explain the features of S2.

Finally, the salient dynamics of the disturbance may be explained by an internal bore under the influence of background rotation, or Kelvin shocks (Helfrich et al. 1999). Helfrich et al. (1999) examine the nonlinear dynamics of Kelvin shocks and show that the largest

TABLE 1. Parameter and estimated uncertainty values for H_1, H_2, θ_1, and θ_2 in the simulation for the 12 Jul feature (S2) at Los Mochis and the surge at Bahia Kino (BK) and Puerto Penasco (PP).

	H_1	H_2	θ_1	θ_2
12 Jul (S2)	1500 ± 120 m	1750 ± 80 m	304.1 ± 0.2 K	308.0 ± 0.5 K
Surge at BK	950 ± 90 m	1430 ± 220 m	304.3 ± 0.2 K	307.5 ± 0.5 K
Surge at PP	470 ± 30 m	1030 ± 70 m	304.4 ± 0.5 K	308.5 ± 0.5 K

perturbation heights and along-coast velocities are at the coast (in agreement with simulated S2; cf. Fig. 5). They also show that as geostrophic adjustment begins to take place, nonzero across-coast velocities are present. Assuming our disturbance can be considered a Kelvin shock, the estimated phase speed of S2 would be [using a nondimensional channel width $w \approx 1$–2 (where w is nondimensionalized by the Rossby radius of deformation), appropriate for the GoC, and initial downstream fluid depth $d_o \approx 0.85$ of the upstream depth (behind shock, d_o is the ratio of the downstream depth to the upstream depth), Helfrich et al. (1999)'s Fig. 21] $14.8 \pm 1.6\,\mathrm{m\,s^{-1}}$, which is close to the modeled phase speed of $16.1\,\mathrm{m\,s^{-1}}$. With respect to the intensity of the Kelvin shock, the structure of the overlying atmosphere as measured by the Scorer parameter is relevant (Crook 1986). The Scorer parameter is a measure of the ability of the atmosphere to trap upward-propagating wave energy (Scorer 1949). It includes two terms, a term related to static stability and a term related to wind profile curvature. If the Scorer parameter is larger than the square of the horizontal wavenumber k^2, upward propagation occurs. For S2, the Scorer parameter is nearly constant with height, around $1.0 \times 10^{-6}\,\mathrm{m^{-2}}$ (Fig. 6), which is larger than waves with horizontal wavelengths >9 km. Hence, vertical trapping of the disturbance is possibly minimal via the theory of Scorer (1949) and simulations of bore-type disturbances in Crook (1986). In the simulation, S2 loses amplitude with time (Fig. 4) agreeing with the theoretical evolution of an internal bore. Including the simulated features indicating rotational impacts and phase speed agreement the Kelvin shock most completely describes the dynamics of S2.

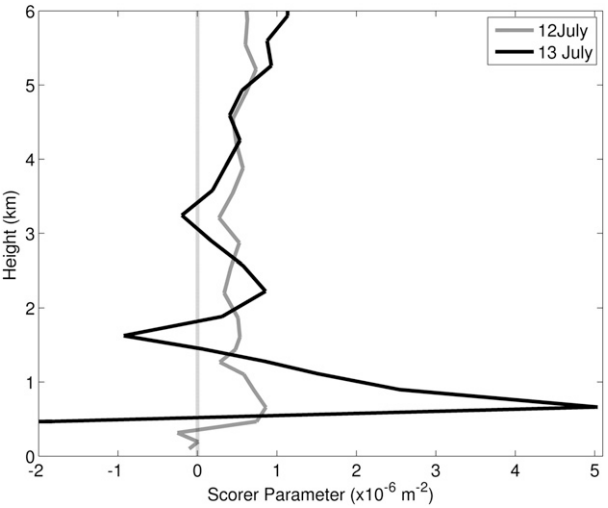

FIG. 6. Vertical profile of the Scorer parameter at 1300 UTC 12 Jul ahead of S2 (solid gray line) and at 0600 UTC 13 Jul (black line) ahead of the surge.

b. Gulf surge

1) INITIATION PHASE

The surge feature on 13 July is very complex with many subtle features. Initially, an increase in flow from convectively cooled air associated with the outer bands of TS Blas near the mouth of the GoC enhances the climatological cool dome over the southern GoC after the passage of S2. Figure 7 displays a CS along AC2 at 0000 UTC 12 July, and 0000 UTC and 0500 UTC 13 July, showing the buildup of the cool dome and encroachment of Pacific air into the GoC that impinges upon the cool inflow from the mouth of the GoC in this case (NJ12). In response to this cool dome build up, surface pressure rises occur at LM between 0100 and 0600 UTC (not shown) and the surge begins to propagate northward (NJ12).

To estimate the modeled total speed of the surge between LM and BK, four different criteria were used. First, the movement of the 2D centroid of the 950-hPa moisture flux maximum was estimated between 0500 and 0900 UTC. The time difference of maximum moisture flux, maximum wind centroid, and maximum MSLP associated with the surge at LM and BK were used as the second through fourth criteria, respectively. These criteria give a model total surge speed between LM and BK of $22.2 \pm 0.8\,\mathrm{m\,s^{-1}}$. Using a corresponding estimate along-surge flow in the preceding environment of $4.1 \pm 1.5\,\mathrm{m\,s^{-1}}$ at BK, the modeled surge phase speed is $18.1 \pm 1.7\,\mathrm{m\,s^{-1}}$. Around and after 0500 UTC 13 July, substantial convective outflow enters the western coastal plain of Mexico and adjacent GoC along the southern and central GoC as the formative surge feature begins to propagate northward (Fig. 8; NJ12). These outflow impingements on the formative surge produce discrete propagation in its formative stages by generating a new leading edge to the surge by 0700 UTC (Fig. 8) and are not accounted for by any of the theory discussed herein.

At BK, there are multiple features on 13 July of which the gulf surge is the last. Briefly, the first feature (0000 UTC 13 July) coinciding with an MSLP anomaly increase, temperature decrease (Fig. 9), and wind shift is associated with the simulated sea-breeze front moving over BK. The increased wind anomaly around 0600–0800 UTC can be tied to a convective cluster along the central SMO. During passage of it over BK, there is an increase in wind anomaly to around $3\,\mathrm{m\,s^{-1}}$ along with a minimal MSLP rise, upward vertical velocities on the leading edge and slight cooling above the surface (Fig. 9). These characteristics suggest this is an internal bore that passes BK (Haertel et al. 2001; Knupp 2006; Martin and Johnson 2008).

The surge begins to pass over BK around 0830–0900 UTC (Fig. 9; NJ12). It is accompanied by a wind

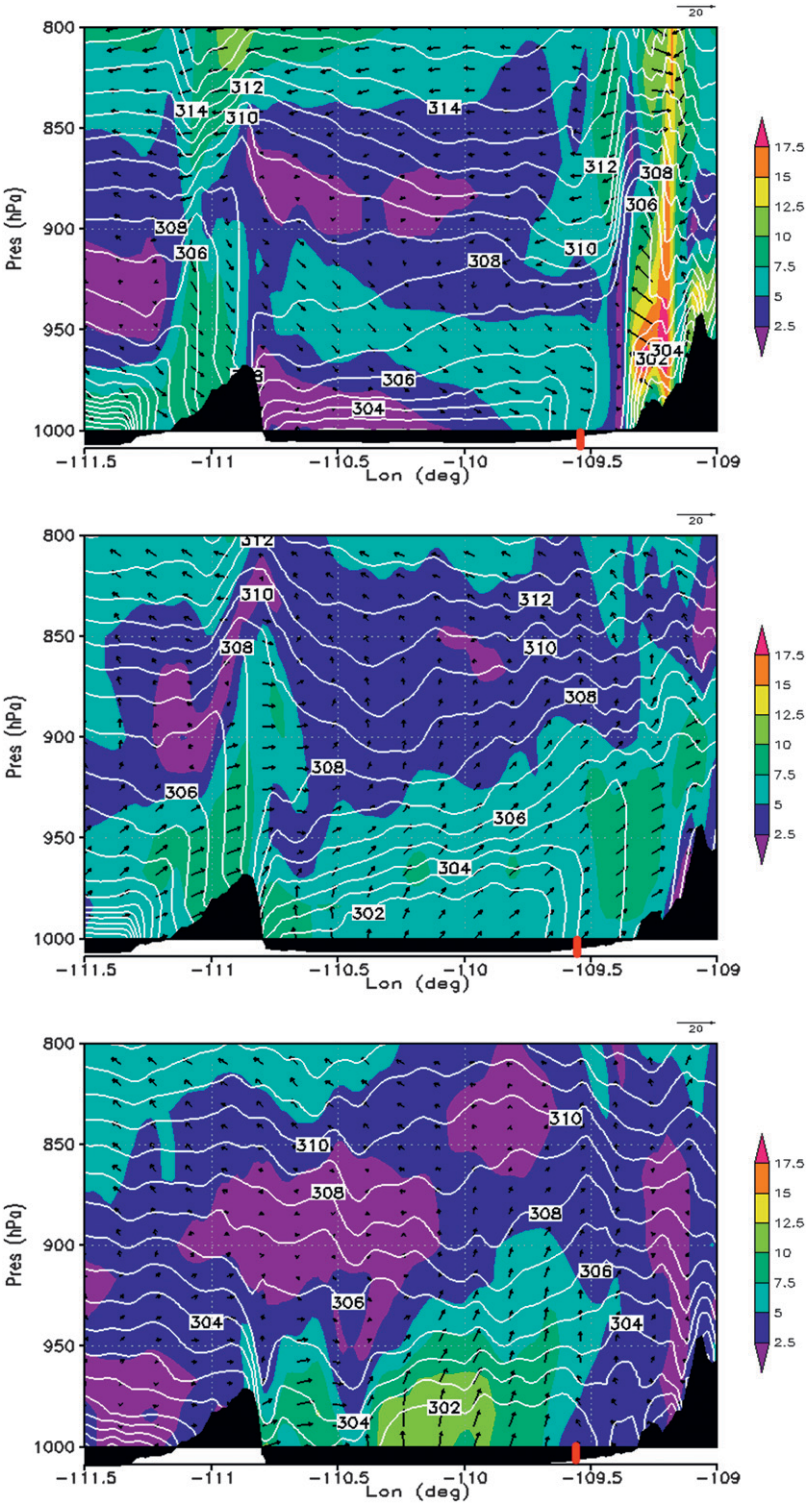

FIG. 7. Simulated potential temperature (K, white contours), wind magnitude (m s^{-1}, shading), and coast-relative wind vectors (arrows) taken along across-gulf cross section AC2 (Fig. 2) at (top) 0000 UTC 12 Jul, (middle) 0000 UTC 13 Jul, and (bottom) 0500 UTC 13 Jul. Black shading indicates topography, while the red line indicates the coastline.

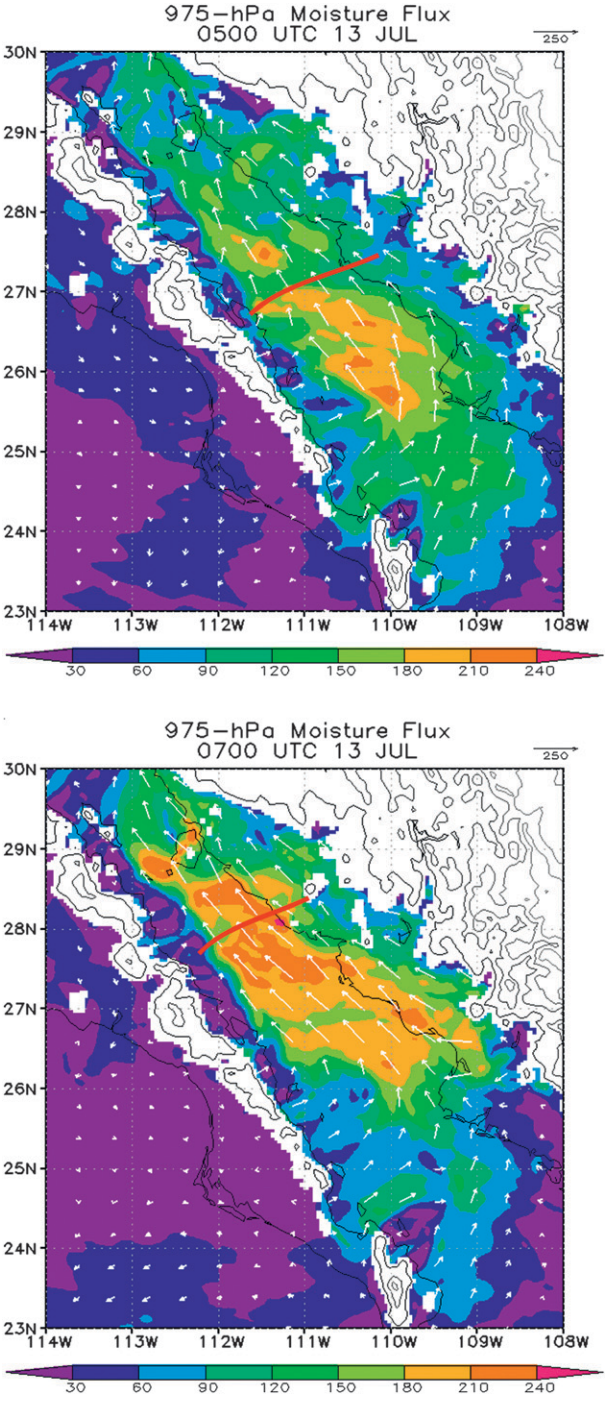

FIG. 8. 975-hPa moisture flux ($g\,m\,kg^{-1}\,s^{-1}$) at (top) 0500 and (bottom) 0700 UTC 13 Jul. The red lines denote the approximate position of the surge leading edge.

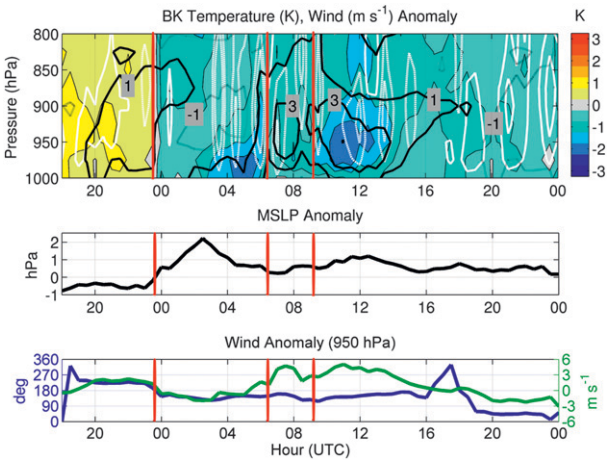

FIG. 9. (top) Bahia Kino temperature anomalies (K, shading), wind anomalies ($m\,s^{-1}$, black contours), and vertical velocity ($Pa\,s^{-1}$, white contours: thin dashed upward, thick solid downward, contour interval $0.5\,Pa\,s^{-1}$). (middle) MSLP anomalies (hPa). (bottom) 950-hPa wind speed ($m\,s^{-1}$) and direction anomalies (°). All panels are anomalies compared to the diurnal mean for the WRF simulation period from 0000 UTC 12 Jul to 0000 UTC 14 Jul and display 1800 UTC 12 Jul–0000 UTC 14 Jul. Red vertical lines denote the passage of the sea breeze, a minor bore, and the gulf surge event in chronological order.

speed increase, cooling through a deeper layer and an anomalous surface pressure increase (Fig. 9) all in phase with each other. Upward vertical velocities are also present at the leading edge of the positive wind and negative temperature anomalies (Fig. 9). The top of the surge at BK is estimated to be 308 K (~1500 m) using the vertical extent of significant wind anomalies, cooling and moistening with the surge [Figs. 9 and 10 (at 1100 UTC)], which is also near the top of the SMO. Again the lowest 200 hPa of the atmosphere is continuously stratified with no clear mixed and inversion layer present (Figs. 10 and 11) and has a mean Brunt–Väisälä frequency of $\sim 0.01\,s^{-1}$. The surge winds are maximized near and inland of the coast with isentropes that intersect the land and slope toward the surface moving away from the SMO, relevant to CTDs of any type. Finally, the wind and MSLP anomalies associated with the surge occur for approximately 5 h (Fig. 9), implying an estimated wavelength of ~650 km.

As with S2, the generation mechanism, large phase speed and short wavelength rule out topographically trapped Rossby waves as the dynamical mechanism for the surge and will not be discussed further. Gravity currents are integral in the development of the initial surge, and would generate in phase positive wind, pressure, and negative temperature anomalies. The estimated maximum phase speed of a gravity current at BK is $\sim 17\,m\,s^{-1}$ using a $\Delta\theta$ of 3 K and a cold pool height of 1500 m. However, the anomalous surface cooling is rather weak and occurs several hours after the initial passage of the surge over BK. Also the maximum wind and most negative temperature anomalies are centered above the surface. These factors suggest that the phenomenon is not a gravity current.

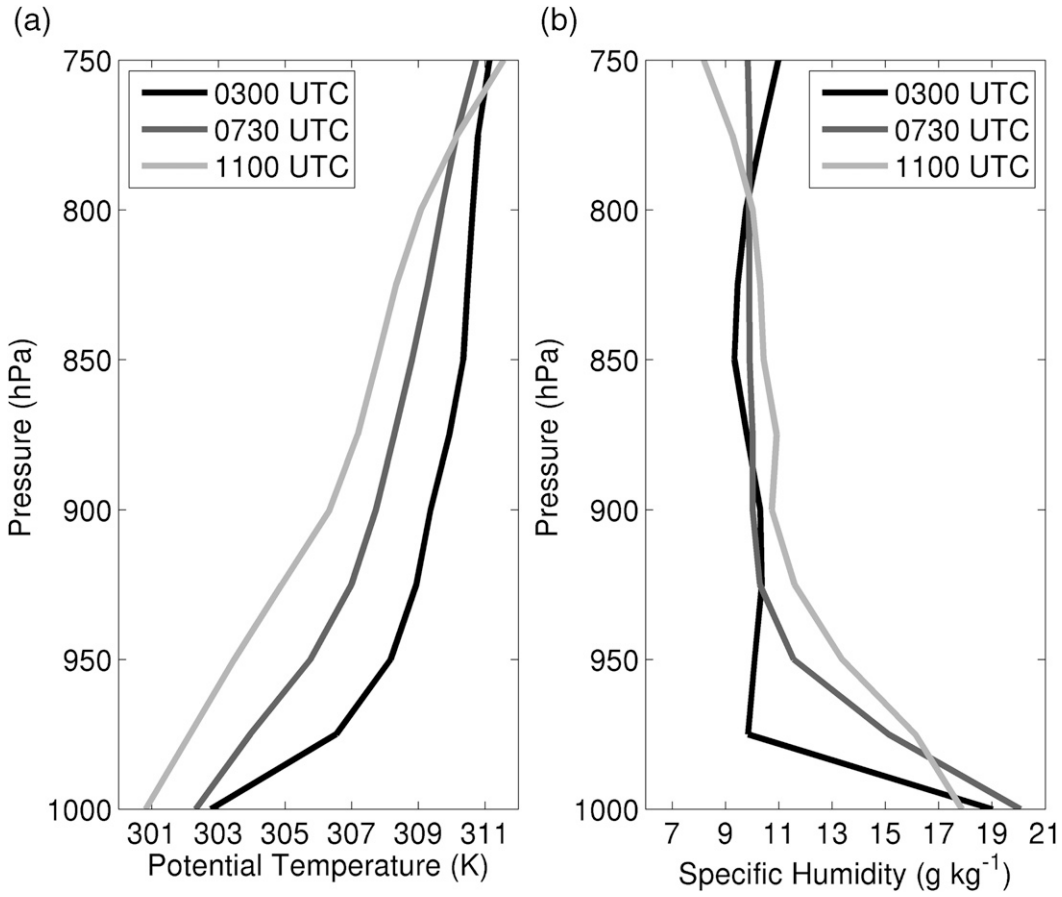

FIG. 10. (a) Potential temperature (K) and (b) mixing ratio ($g\,kg^{-1}$) for the surge event at Bahia Kino at 0300 (black), 0730 (medium gray), and 1100 (light gray) UTC 13 Jul.

Multiple factors argue against a Kelvin wave interpretation. Stratification without a clear inversion layer precludes inversion-trapped Kelvin waves while linear step-trapped Kelvin waves would have a phase speed of $\sim 9\,m\,s^{-1}$, half that of the modeled surge. The surge at BK is likely not subinertial, with an angular frequency of $\omega_s \approx 1.4 \times 10^{-4}$, larger than Corilois at 30°N ($7.3 \times 10^{-5}\,s^{-1}$). Additionally, there are nonnegligible across-coast velocities within the surge (Fig. 11).

The above considerations lead to the conclusion that the surge at this stage can best be explained in terms of bore dynamics. The theoretical phase speed of an internal bore at BK is $C_B \approx 13.2 \pm 4.8\,m\,s^{-1}$ while that of a Kelvin shock is $\sim 12.8 \pm 4.8\,m\,s^{-1}$ (Tables 1 and 2). These phase speeds are about $5\,m\,s^{-1}$ slower than that of the modeled surge, likely due to discrete propagation of the surge in its formative stages. As noted above and in NJ12, multiple convective outflows impinge on the southern and central GoC between 0500 and 0800 UTC. These outflows generate a new leading edge to the surge by 0700 UTC (Fig. 8), which impacts the total system speed in a way that is not accounted for by the theory used herein. Overall, the Kelvin shock is the best dynamical fit for the surge at BK; it can account for the generation mechanism, wind maximum, potential temperature slope, and across-coast flow. Focus will now shift to the mature phase of the surge as simulated between BK and Puerto Penasco (PP).

2) MATURE PHASE

As at BK, more than one feature passes over PP. The first two features are generated by convective outflow from two convective clusters along the northern SMO (NJ12). A weak feature passage, consistent with that of a gravity current (Simpson 1997; Haertel et al. 2001), is modeled with an MSLP rise beginning around 0100 UTC, an associated wind speed increase by 0200 UTC, low-level and surface cooling, and an MSLP rise (Fig. 12) and is the first of three distinct feature passages at PP. The second feature passes over PP from 0500 to 0800 UTC and has cooling centered around 975 hPa, an MSLP anomaly rise between 0600 and 0830 UTC, and the

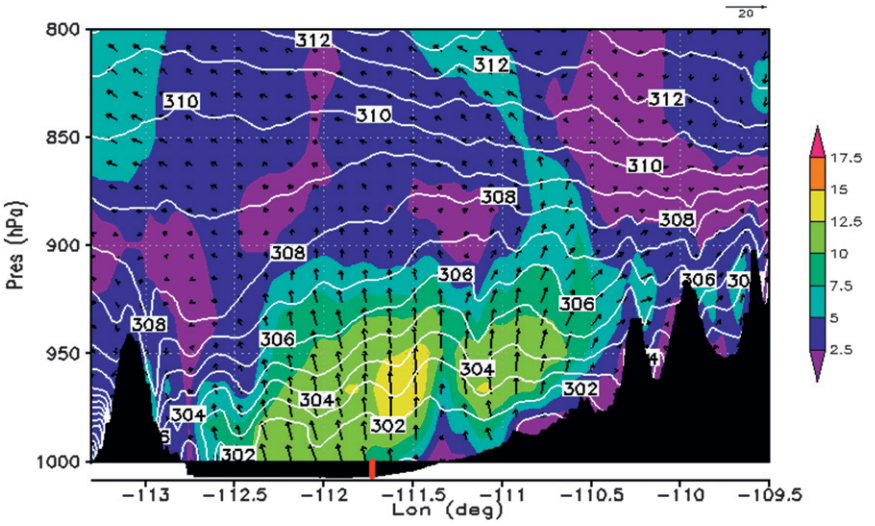

FIG. 11. Simulated potential temperature (K, white contours), wind magnitude ($m\,s^{-1}$, shading), and coast-relative wind vectors (arrows) taken along across-gulf cross section AC3 (Fig. 2) at 1000 UTC 13 Jul. Black shading indicates topography, while the red line indicates the coastline.

initial wind anomaly increase occurs near 975 hPa (Fig. 12, 0830 UTC). These characteristics are consistent with the passage of an internal bore (Haertel et al. 2001; Knupp 2006; Martin and Johnson 2008).

There is a small break period after the 0500–0800 UTC bore passage noted by the decrease in the wind and MSLP anomaly just before 0900 UTC (Fig. 12) before the surge feature begins to impact PP. After 0900 UTC a more significant increase in the near-surface negative temperature anomalies is visible through ~1800 UTC, centered at 975–950 hPa with a maximum after ~1200 UTC (Fig. 12). This feature is the modeled surge passing over PP. The surge is associated with in-phase positive wind and MSLP anomalies and negative temperature anomalies that slightly lag. There are also several regions of upward motion throughout the surge (Fig. 12). Surge cross sections AC3 and AG2 highlight across-coast flow (Fig. 13), isentropes that intersect the terrain (Fig. 13) and slope downward away from the SMO, and maximum wind anomalies collocated with the most negative temperature anomalies (Fig. 14). Also, there is a distinct transition to more positive along CS winds (southeasterly meteorological winds) and more negative temperature anomalies, both of which are maximized around 975–950 hPa and deepen behind the leading edge of the surge as it approaches PP (Fig. 14). Between BK and PP (320 km), the movement of the modeled surge was estimated using the same four criteria as between LM and BK. These criteria give an estimated total surge speed of $20.4 \pm 1.4\,m\,s^{-1}$ between BK and PP. The along-surge flow is estimated at $7 \pm 1.5\,m\,s^{-1}$, resulting in a modeled surge phase speed of $13.4 \pm 2.1\,m\,s^{-1}$. The positive southerly wind anomalies occur for ~10–12 h at PP (Fig. 12) giving an estimated wavelength of ~1100 km and an angular frequency of $\omega_s \approx 7.7 \times 10^{-5}\,s^{-1}$.

The lack of strong surface cooling and positive wind anomalies exclude gravity currents as the likely dynamical mechanism for the surge in the northern GoC, although they may play a role in amplifying the overall disturbance. Also, coastally trapped Kelvin waves can be disqualified as the dynamical mechanism. Assuming a surge top of 308.5 K (Table 1), linear shallow-water Kelvin waves trapped by an inversion layer would have a phase speed of $7.8 \pm 1.2\,m\,s^{-1}$, while step-trapped Kelvin waves would have a phase speed of ~8–9 $m\,s^{-1}$ again. These speeds are 4–5 $m\,s^{-1}$ slower than modeled and outside the uncertainty bounds. Also, the surge at PP may not be subinertial ($\omega_s \approx 7.7 \times 10^{-5}\,s^{-1}$, $f \approx 7.3 \times 10^{-5}\,s^{-1}$ at 30°N) and there is a net northward moisture transport to the northern GoC (NJ12), which is not possible with linear Kelvin waves (Zehnder 2004). Finally, nonlinear Kelvin waves would have a phase speed only slightly slower than modeled (~12 $m\,s^{-1}$ for shallow-water-type Kelvin waves; Ralph et al. 2000); however,

TABLE 2. Simulated and theoretical phase speeds and estimated uncertainty for the 12 Jul feature (S2) at Los Mochis and the surge at Bahia Kino (BK) and Puerto Penasco (PP); C_{WRF}, C_{STKW}, and C_B are the modeled-estimated, step-trapped Kelvin wave, and internal bore phase speeds, respectively.

	C_{WRF}	C_{STKW}	C_B
12 Jul (S2)	$16.1 \pm 1.9\,m\,s^{-1}$	$8.5 \pm 1.5\,m\,s^{-1}$	$15.3 \pm 1.6\,m\,s^{-1}$
Surge at BK	$18.1 \pm 1.7\,m\,s^{-1}$	$8.5 \pm 1.5\,m\,s^{-1}$	$13.2 \pm 4.8\,m\,s^{-1}$
Surge at PP	$13.4 \pm 2.1\,m\,s^{-1}$	$8.5 \pm 1.5\,m\,s^{-1}$	$13.6 \pm 2.4\,m\,s^{-1}$

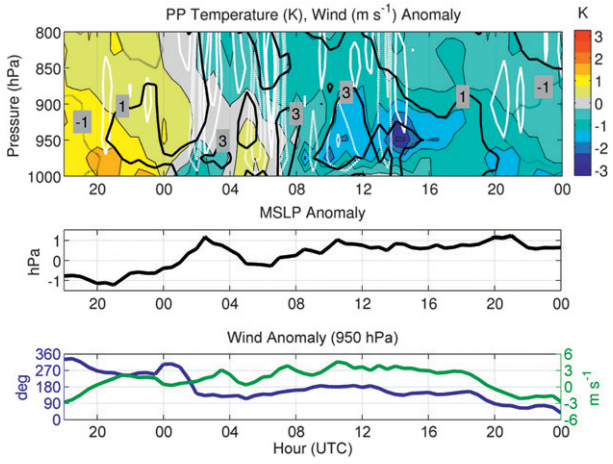

FIG. 12. (top) PP temperature anomalies (K, shading), wind anomalies ($m\,s^{-1}$, black contours), and vertical velocity ($Pa\,s^{-1}$, white contours: dashed upward, contour interval $0.5\,Pa\,s^{-1}$). (middle) MSLP anomalies (hPa). (bottom) 950-hPa wind speed ($m\,s^{-1}$) and direction anomalies (°). All panels are anomalies compared to the diurnal mean for the WRF simulation period 0000 UTC 12 Jul–0000 UTC 14 Jul and display 1800 UTC 12 Jul–0000 UTC 14 Jul.

the extent of across-coast flow present (Fig. 13) is not accounted for by coastally trapped Kelvin wave theory (Reason and Steyn 1992).

Kelvin shocks or internal bores modified by rotation are the best dynamical match for the surge in the northern GoC. The phase speed for an internal bore at PP is $C_B \approx 13.6 \pm 2.4\,m\,s^{-1}$ and a Kelvin shock is $\sim 13.2 \pm 2.4\,m\,s^{-1}$ (Table 2). Including the along-surge flow results in total speeds of 20.2–20.6 $\pm$ $2.4\,m\,s^{-1}$, corresponding very well with the modeled surge total speed. Additionally, the Kelvin shock solution explains the intersecting isentropes along the SMO and the decay away from the SMO, the wind maximum near the coast, and can account for some of the across-coast flow modeled. Interestingly, the estimated phase speed for an internal bore at BK agrees with the modeled phase speed estimate between BK and PP as well. This suggests the surge has fully developed by BK and is one dynamical feature throughout the central and northern GoC.

Finally, on 13 July the Scorer parameter has two areas of distinct decrease with height, −0.75–1.5 and 0.2–3.2 km (Fig. 6). The lower layer is related to the GoC low-level jet and the top of the boundary layer, while the second layer has coincident areas of decreasing stability and increasing wind curvature with height, which implies that the environment on 13 July is conducive to gravity wave trapping or internal bores (Crook 1986). An environment suitable for internal bore propagation on 13 July and not 12 July explains the inability of S2 to propagate into the northern GoC and its loss of amplitude with northward extent. The surge on 13 July is able to maintain its amplitude and intensity while traveling over 300 km as a result of the favorable environment for bore propagation without energy loss (Crook 1986).

One complicating factor in this analysis is that at the northern end of the gulf, the topography fans out tremendously and becomes less continuous (Fig. 2), which could explain the extensive cross-coast flow. In this region, the arguments regarding coastally trapped disturbances are more tenuous. Reason and Steyn (1992) include dissipation because of gaps in topography. Gaps

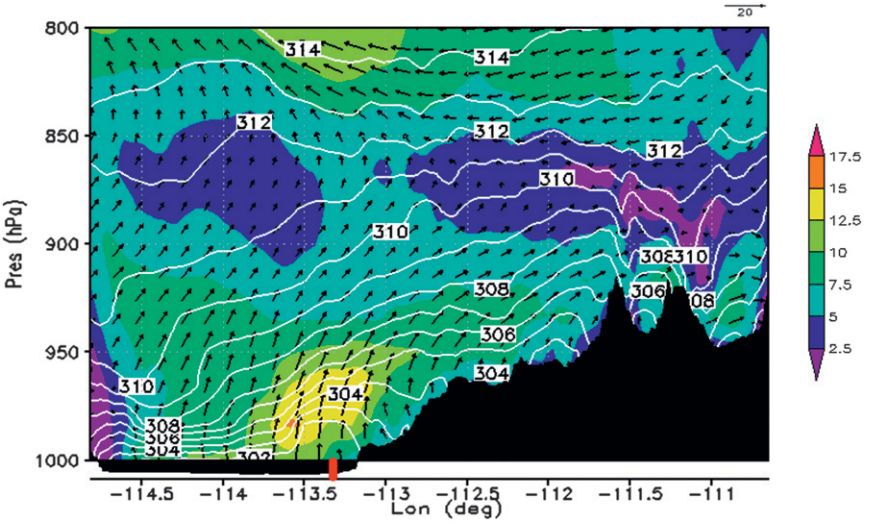

FIG. 13. Simulated potential temperature (K, white contours), wind magnitude ($m\,s^{-1}$, shading), and coast-relative wind vectors (arrows) taken along across-gulf cross section AC4 (Fig. 2) at 1300 UTC 13 Jul. Black shading indicates topography, while the red line indicates the coastline.

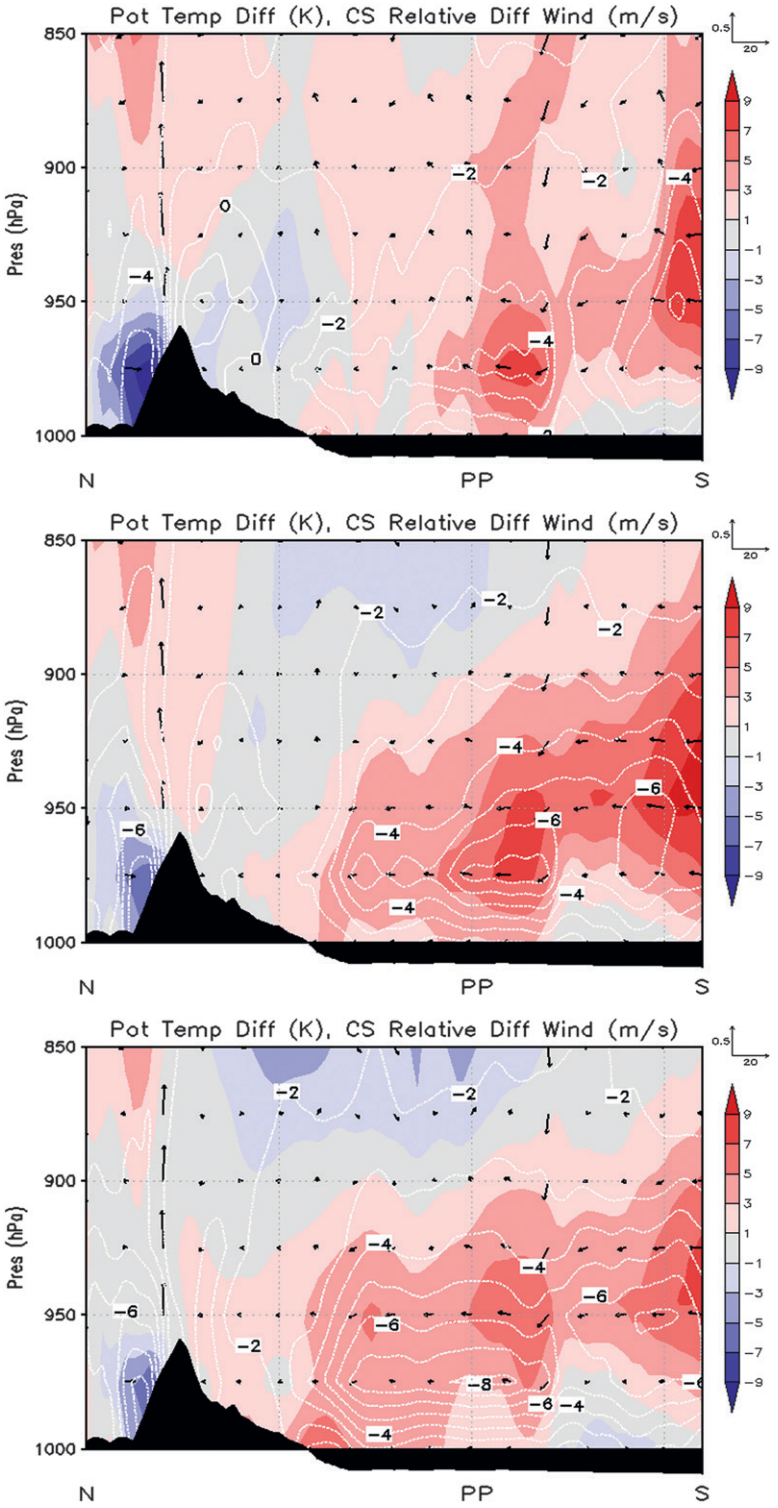

FIG. 14. Potential temperature differences (white contours) and along cross-sectional wind differences (arrows and shading) along AG2 (Fig. 2) on 13 Jul. Differences are taken as (top) 1030–0500 UTC, (middle) 1300–0500 UTC, and (bottom) 1430–0500 UTC.

in the coastal barrier are parameterized via a small across-coast flow component. However, gently sloping terrain with gaps as is seen in the northern GoC (Figs. 2, 11, and 13) is not accounted for by any theory. The sloping topography may allow for across-coast flow via incomplete blocking of the surge event. In any event, the Kelvin shock most favorably accounts for the features of the surge in the northern GoC. Nonideal terrain may then account for the increased across-coast flow.

c. Comparison of modeled to observed surge

The general features of the modeled precursor wave and surge agree qualitatively well with the observed as reported in NJ12. A convectively generated gravity current initiates the precursor Kelvin shock on 12 July in both the observations and model. Multiple convective clusters in the southern GoC on early 13 July generate various convective outflows that interact with the formative surge over the southern GoC as observed (NJ12), indicating that the model simulation captures the dynamics of surge initiation. While the theoretical phase and total system speeds increase between BK and PP (Table 2), the modeled surge speed decreases from 22.4 ± 0.8 to $20.4 \pm 1.4\,\mathrm{m\,s^{-1}}$ between the LM–BK and BK–PP legs, which is in general agreement with observations (RJ07). The presurge and surge features at BK, a stronger surge feature at PP, and a slight lag in moisture flux increases at BK and PP are all present in RJ07. The height of the surge top decreases about 400 m with northward extent, which is also in agreement with observations.

As discussed in NJ12 the depth of the high winds and largest cooling associated with the modeled surge are too shallow. However, when examining Fig. 12 of RJ07, the top of the inversion is at a similar height (~900 hPa) and temperature (309 K) to that of the modeled surge. The wind field in RJ07 is much stronger throughout the troposphere over the course of the observed surge event, suggesting the model is not capturing some other process(es) (e.g., the modeled maximum large-scale MSLP pressure gradient between LM and PP is 2.4 hPa less than observed). The core of the modeled surge near PP is at roughly 950 hPa, which does agree well with the observed surge. However, there is modeled wind bias (model minus observation) of almost $-4\,\mathrm{m\,s^{-1}}$ between 0800 and 1800 UTC 13 July, during the core time of the surge event. Addition of that bias to the modeled wind field would give the appearance of a much deeper surge event, in better agreement with the observations. The similarity of the modeled surge to that observed including the model wind bias provides further evidence that a Kelvin shock can explain both the modeled and observed surge on 13 July 2004.

4. Summary

A high-resolution simulation of a gulf surge event during the North American Monsoon Experiment is examined herein to determine the dynamical evolution of the surge feature. The simulation provides a good representation of the features of the surge event (NJ12). Comparisons to the theoretical characteristics of topographically trapped Rossby waves, gravity currents, Kelvin waves, and internal bores are made to diagnose the dynamical mechanisms of the precursor wave and the surge event. Overall, the entire event is complex with many subtle features and convective episodes.

a. Simulated surge description

Initially, convection associated with the tropical easterly wave (TEW) precursor to Tropical Storm (TC) Blas creates a convective cluster in the southern Gulf of California (GoC) around 0600–0900 UTC 12 July. This cluster interacts with the climatological cool dome to create an internal bore that propagates up the GoC, slowly moves ahead of the dissipating gravity current, and becomes diffuse just south of Bahia Kino (BK) around 2200 UTC 12 July (feature labeled S2 in the text). Southerly flow, moistening, and slight cooling below are present in the simulation behind the wave. Convection then forms along the length of the Sierra Madre Occidental (SMO) late on 12 July into 13 July. Inflow from the mouth of the GoC and Pacific Ocean along with convective outflow impinging on the southern GoC initiates the surge feature by early on 13 July. Continued convective outflow entering the GoC intensifies the surge as it propagates up the GoC. As the core of the surge passes through BK and Puerto Penasco (PP), it is most likely an internal bore influenced by the earth's rotation or a *Kelvin shock* after Helfrich et al. (1999). Substantial low-level cooling and moistening are associated with the simulated surge feature as observed.

That the surge signal seen at PP on 13 July is preceded by a wave on 12 July associated with a TEW could possibly explain how TEW/TCs are tied to gulf surge events. Stensrud et al. (1997), Fuller and Stensrud (2000), and Adams and Stensrud (2007) show that gulf surges are typically preceded by TEW passage. Adams and Stensrud (2007) also find that removal of TEWs in a simulation results in weaker surges that occur at different times and are often associated with waves generated internally by the model. In this case, removal of the bore on 12 July may change the evolution and character of the surge event on 13 July since it is followed by cooling, moistening, and southerly flow in the southern and central GoC that extend into 13 July. It could be that without this initial cooling and inflow into the southern GoC,

the surge and convective initiation and evolution along the southern SMO would be different. This should be the subject of further study.

b. Surge dynamics

The features associated with the disturbance on 12 July (labeled S2) indicate that it is an internal bore/Kelvin shock that moves ahead of the dissipating initiating gravity current (S1) with minimal surface cooling, nonzero across-coast flow, isentropes that intersect the SMO, and maximum winds and lowest potential temperatures near the coastline. S2 decays with time as it moves along the GoC, washing out just south of BK around 2000–2200 UTC. The vertical profile of the Scorer parameter just ahead of S2 (Fig. 6) shows no trapping layer above indicating that the modeled decay is at least partially due to vertical energy loss.

On 13 July the initial surge forms through a consolidation of cool air moving into the GoC from near the mouth, along with convective outflows from the west slopes of the SMO impinging on the coastal plain around 0500 UTC 13 July. As the surge moves up the GoC, many convective outflows, either gravity currents or bores, impinge upon the GoC near and ahead of the initial Kelvin wave, causing enhancement and deepening of the cool anomaly. The surge begins to impact BK around 0830 UTC 13 July (Fig. 9). The modeled surge has a total system speed of $\sim 22\,\mathrm{m\,s^{-1}}$ in the southern and central GoC, which is faster than all theoretical estimates for the surge at BK ($\sim 17\,\mathrm{m\,s^{-1}}$ for a Kelvin shock; Table 2). This is due to the impinging outflows creating a new surge leading edge around 0700 UTC in the central GoC, increasing the surge system speed between LM and BK in a way not accounted for by the steady propagation used in the formulation of phase speeds for Kelvin shocks (Helfrich et al. 1999).

At PP the gulf surge is preceded by two weak features, both generated by convective clusters decaying along the northern SMO. When the surge reaches PP it has a modeled total system speed of $20.4 \pm 1.4\,\mathrm{m\,s^{-1}}$. The theoretical phase speed estimate for a Kelvin shock is $13.2 \pm 2.4\,\mathrm{m\,s^{-1}}$, while it is $13.4 \pm 2.1\,\mathrm{m\,s^{-1}}$ for the observed surge (Table 2). This, along with the modeled features of maximum above-surface cooling, a positive MSLP anomaly, isentropes that intersect the SMO and decay toward the surface away from the SMO, maximum wind velocities near the coast, and nonzero across-coast flow support the argument that the modeled surge at PP is a Kelvin shock, or an internal bore modified by rotation and bounded on the right by the SMO.

Acknowledgments. The authors thank Paul Ciesielski, Brian McNoldy, and Rick Taft for their assistance relating to this research. The authors would also like to thank two anonymous reviewers and Editor Dale Durran for greatly improving this manuscript. This work was supported by NASA Headquarters through NASA Grants NNX07AD35G and NNX10AG81G, and by the National Science Foundation, by both the Mesoscale Dynamic Meteorology Program, under Grant ATM-0639461, and the Physical and Dynamic Meteorology Program, under Grant AGS-0966758. Finally, we would like to acknowledge high-performance computing support provided by NCAR's Computational and Information Systems Laboratory, sponsored by the National Science Foundation.

REFERENCES

Adams, J. L., and D. J. Stensrud, 2007: Impact of tropical easterly waves on the North American monsoon. *J. Climate,* **20,** 1219–1238.

Anderson, B. T., J. O. Roads, and S.-C. Chen, 2000a: Large-scale forcing of summertime monsoon surges over the Gulf of California and the southwestern United States. *J. Geophys. Res.,* **105** (D19), 24 455–24 467.

——, ——, ——, and H.-M. H. Juang, 2000b: Regional simulation of the low-level monsoon winds over the Gulf of California and southwestern United States. *J. Geophys. Res.,* **105** (D14), 17 955–17 969.

Benjamin, T. B., 1968: Gravity currents and related phenomena. *J. Fluid Mech.,* **31,** 209–248.

Berbery, E. H., 2001: Mesoscale moisture analysis of the North American Monsoon. *J. Climate,* **14,** 121–137.

Bordoni, S., and B. Stevens, 2006: Principal component analysis of the summertime winds over the Gulf of California: A gulf surge index. *Mon. Wea. Rev.,* **134,** 3395–3414.

Brenner, I. S., 1974: A surge of maritime tropical air—Gulf of California to the southwestern United States. *Mon. Wea. Rev.,* **102,** 375–389.

Bruyere, C., and Coauthors, 2010: Weather Research and Forecasting ARW version 3 modeling system user's guide. Mesoscale & Microscale Meteorology Division, National Center for Atmospheric Research, 312 pp. [Available from the National Center for Atmospheric Research, Boulder, CO 80301.]

Bryan, G. H., and H. Morrison, 2012: Sensitivity of a simulated squall line to horizontal resolution and parameterization of microphysics. *Mon. Wea. Rev.,* **140,** 202–225.

Crook, N. A., 1986: The effect of ambient stratification and moisture on the motion of atmospheric undular bores. *J. Atmos. Sci.,* **43,** 171–181.

Dorman, C., 1985: Evidence of Kelvin waves in California's marine layer and related eddy generation. *Mon. Wea. Rev.,* **113,** 827–839.

——, 1987: Possible role of gravity currents in northern California's coastal summer wind reversals. *J. Geophys. Res.,* **92** (C2), 1497–1506.

Douglas, M. W., and J. C. Leal, 2003: Summertime surges over the Gulf of California: Aspects of their climatology, mean structure, and evolution from radiosonde, NCEP reanalysis, and rainfall data. *Wea. Forecasting,* **18,** 55–74.

Durran, D. R., 2000: Small-amplitude coastally trapped disturbances and the reduced-gravity shallow-water approximation. *Quart. J. Roy. Meteor. Soc.,* **126,** 2671–2689.

Federov, A. V., and W. K. Melville, 1996: Hydraulic jumps at boundaries in rotating fluids. *J. Fluid Mech.,* **324,** 55–82, doi:10.1017/S0022112096007835.

Fuller, R. D., and D. J. Stensrud, 2000: The relationship between tropical easterly waves and surges over the Gulf of California during the North American monsoon. *Mon. Wea. Rev.,* **128,** 2983–2989.

Gill, A. E., 1977: Coastally trapped waves in the atmosphere. *Quart. J. Roy. Meteor. Soc.,* **103,** 431–440.

——, 1982: *Atmosphere-Ocean Dynamics.* Academic Press, 662 pp.

Gochis, D. J., A. J. Jimenez, C. J. Watts, J. Garatuza-Payan, and W. J. Shuttleworth, 2004: Analysis of 2002 and 2003 warm season precipitation from the North American Monsoon Experiment event rain gauge network. *Mon. Wea. Rev.,* **132,** 2938–2953.

Haertel, P. T., R. H. Johnson, and S. N. Tulich, 2001: Some simple simulations of thunderstorm outflows. *J. Atmos. Sci.,* **58,** 504–516.

Hales, J. E., Jr., 1972: Surges of maritime tropical air northward over the Gulf of California. *Mon. Wea. Rev.,* **100,** 298–306.

Helfrich, K. R., A. C. Kuo, and L. J. Pratt, 1999: Nonlinear Rossby adjustment in a channel. *J. Fluid Mech.,* **390,** 187–222, doi:10.1017/S0022112099005042.

Higgins, R. W., and W. Shi, 2005: Relationships between Gulf of California moisture surges and tropical cyclones in the eastern Pacific basin. *J. Climate,* **18,** 4601–4620.

——, ——, and C. Hain, 2004: Relationships between Gulf of California moisture surges and precipitation in the southwestern United States. *J. Climate,* **17,** 2983–2997.

——, and Coauthors, 2006: The NAME 2004 field campaign and modeling strategy. *Bull. Amer. Meteor. Soc.,* **87,** 79–94.

Holland, G. J., and L. M. Leslie, 1986: Ducted coastal ridging over S.E. Australia. *Quart. J. Roy. Meteor. Soc.,* **112,** 731–748.

Klemp, J. B., R. Rotunno, and W. C. Skamarock, 1997: On the propagation of internal bores. *J. Fluid Mech.,* **331,** 81–106.

Knupp, K., 2006: Observational analysis of a gust front to bore to solitary wave transition within an evolving nocturnal boundary layer. *J. Atmos. Sci.,* **63,** 2016–2035.

Maddox, R. A., D. M. McCollum, and K. W. Howard, 1995: Large-scale patterns associated with severe summertime thunderstorms over central Arizona. *Wea. Forecasting,* **10,** 763–778.

Maloney, E. D., and D. L. Hartmann, 2000: Modulation of eastern North Pacific hurricanes by the Madden–Julian oscillation. *J. Climate,* **13,** 1451–1460.

Martin, E. R., and R. H. Johnson, 2008: An observational and modeling study of an atmospheric internal bore during NAME 2004. *Mon. Wea. Rev.,* **136,** 4150–4167.

Mass, C. F., and M. D. Albright, 1987: Coastal southerlies and along-shore surges of the west coast of North America: Evidence of mesoscale topographically trapped response to synoptic forcing. *Mon. Wea. Rev.,* **115,** 1707–1738.

Mejia, J. F., M. W. Douglas, and P. J. Lamb, 2010: Aircraft observations of the 12–15 July 2004 moisture surge event during the North American Monsoon Experiment. *Mon. Wea. Rev.,* **138,** 3498–3513.

Mesinger, F., and Coauthors, 2006: North American Regional Reanalysis. *Bull. Amer. Meteor. Soc.,* **87,** 343–360.

Newman, A., and R. H. Johnson, 2012: Simulation of a North American monsoon gulf surge event and comparison to observations. *Mon. Wea. Rev.,* **140,** 2534–2554.

Ralph, F. M., P. J. Neiman, P. O. G. Persson, J. M. Bane, M. L. Cancillo, J. M. Wilczak, and W. Nuss, 2000: Kelvin waves and internal bores in the marine boundary layer inversion and their relationship to coastally trapped wind reversals. *Mon. Wea. Rev.,* **128,** 283–300.

Reason, C. J. C., and D. G. Steyn, 1992: The dynamics of coastally trapped ridges in the lower atmosphere. *J. Atmos. Sci.,* **49,** 1677–1692.

Rogers, P. J., and R. H. Johnson, 2007: Analysis of the 13–14 July gulf surge event during the 2004 North American Monsoon Experiment. *Mon. Wea. Rev.,* **135,** 3098–3117.

Rogerson, A. M., and R. M. Samelson, 1995: Synoptic forcing of coastal-trapped disturbances in the marine atmospheric boundary layer. *J. Atmos. Sci.,* **52,** 2025–2040.

Rottman, J. W., and J. E. Simpson, 1989: The formation of internal bores in the atmosphere: A laboratory model. *Quart. J. Roy. Meteor. Soc.,* **115,** 941–963.

Scorer, R. S., 1949: Theory of waves in the lee of mountains. *Quart. J. Roy. Meteor. Soc.,* **75,** 41–56.

Simpson, J. E., 1997: *Gravity Currents in the Environment and the Laboratory.* Cambridge University Press, 244 pp.

Skamarock, W. C., R. Rotunno, and J. B. Klemp, 1999: Models of coastally trapped disturbances. *J. Atmos. Sci.,* **56,** 3350–3365.

Stensrud, D. J., R. L. Gall, and M. K. Nordquist, 1997: Surges over the Gulf of California during the Mexican monsoon. *Mon. Wea. Rev.,* **125,** 417–437.

Sukoriansky, S., B. Galperin, and V. Perov, 2006: A quasi-normal scale elimination model of turbulence and its application to stably stratified flows. *Nonlinear Processes Geophys.,* **13,** 9–22, doi:10.5194/npg-13-9-2006.

Thompson, G., P. R. Field, R. M. Rasmussen, and W. D. Hall, 2008: Explicit forecasts of winter precipitation using an improved bulk microphysics scheme. Part II: Implementation of a new snow parameterization. *Mon. Wea. Rev.,* **136,** 5095–5115.

Zehnder, J. A., 2004: Dynamic mechanisms of the Gulf surge. *J. Geophys. Res.,* **109,** D10107, doi:10.1029/2004JD004616.